Shock Waves (2020) 30:13–27
https://doi.org/10.1007/s00193-019-00904-4

ORIGINAL ARTICLE

A model for the trajectory of the transverse detonation resulting from re-initiation of a diffracted detonation

X. Q. Yuan[1] · X. C. Mi[2] · H. D. Ng[3] · J. Zhou[1]

Received: 20 September 2018 / Revised: 20 April 2019 / Accepted: 29 April 2019 / Published online: 20 May 2019

Abstract
A semi-analytical model is presented for predicting the trajectory of the transverse detonation during the re-initiation process of a diffracted cellular detonation wave from a channel. Numerical simulations based on the two-dimensional reactive Euler equations with a detailed hydrogen/oxygen chemistry model were first performed to observe key characteristics of cellular detonation wave diffraction and to obtain required input parameters for the model construction. The present numerical observations indicate that the transverse detonation stems from a location on the expansion wave front, and the horizontal distance from this initial location to the channel exit can be scaled by a constant multiplied by the detonation cell width for large deviation angles of the channel. The velocity of the transverse detonation basically equals the Chapman–Jouguet detonation wave velocity consisting of two orthogonal components: the expansion velocity of the diffracted wave front and the relative velocity to the diffracted wave front. The shape of the decoupled wave front is not affected by local explosion and thus can be predicted by the Chester–Chisnell–Whitham theory. Based on these numerical observations and the Chester–Chisnell–Whitham theory, a semi-analytical model is constructed to predict the wave trajectories as well as the distances of the wall reflection point for various deviation angles and initial pressures. The model prediction agrees with the corresponding numerical results. The model result shows that the distance of the wall reflection point varies from 15 to 20 multiples of the cell width with a minimal dependence on deviation angle, independent of the initial pressure. The trajectory calculated by the model is self-similar and determined by the horizontal distance of the initial location. The dimensionless trajectories divided by the horizontal distance are coincident for different initial pressures.

Keywords Cellular detonation diffraction · Transverse detonation · Chester–Chisnell–Whitham theory · Semi-analytical model

1 Introduction

When a detonation wave propagates from a confined area into an unconfined volume, the diffraction phenomenon occurs. Affected by the expansion wave originating at the expansion corner, the detonation diffraction may lead to either detonation failure under a subcritical condition, or a successful re-initiation in a supercritical case [1]. Moreover, in a re-initiation process, a new detonation wave propagating transversely along the diffracted wave front will be formed. This transverse detonation plays a major role in re-uniting the decoupled shock front and reaction zone and eventually results in the diffracted detonation wave propagating sustainably in the open area [2].

As a fundamental problem of detonation research, the detonation diffraction phenomenon has been studied by a number of researchers in the past few decades. The early studies generally focused on the critical condition for a successful re-initiation in cellular detonation diffraction. Zeldovich [1] first experimentally determined that the critical tube diameter d_c, the diameter value below which a detonation cannot transmit into an open area, is about $500\Delta_I$ to $700\Delta_I$, where Δ_I represents the length of the detonation induction zone.

Communicated by N. Smirnov.

✉ X. Q. Yuan
yxq_nudt@hotmail.com

[1] Science and Technology on Scramjet Laboratory, National University of Defense Technology, Changsha 410073, China

[2] Department of Mechanical Engineering, McGill University, Montreal, QC H3A 2K6, Canada

[3] Department of Mechanical, Industrial and Aerospace Engineering, Concordia University, Montreal, QC H3G 1M8, Canada

The criterion was then re-expressed in Mitrofanov [3] by using detonation cell width λ as $d_c = 10\lambda$ for a flat channel and $d_c = 13\lambda$ for a cylindrical tube. The critical tube diameter criterion was verified extensively for most common hydrocarbons/O_2/N_2 mixtures by Knystautas et al. [4]. The mechanisms of diffraction and re-initiation under supercritical conditions were also explored in a number of studies. Edwards et al. [2] studied the re-initiation process theoretically, determining the condition for local explosion as well as the position where re-initiation originates. Murray and Lee [5] built a quantitative model for the diffraction and re-initiation process, which supports the theory of Edwards et al. The effect of activation energy on the re-initiation process was also investigated in detail by Arienti and Shepherd [6] and Pintgen and Shepherd [7]. The latter, and also recently Gallier et al. [8], pointed out that the effect of unsteadiness in the reaction process affects the decoupling between the reaction front and the leading diverging shock.

Two mechanisms of detonation diffraction failure were also conjectured by Lee [9]: For highly unstable detonations, the failure is due to the suppression of transverse instabilities by corner expansion; for weakly unstable detonations, an excessive front curvature distributed over the global detonation surface is responsible for the failure. These conjectured mechanisms were experimentally supported by recent findings of Mehrjoo et al. that, for highly unstable mixtures, the critical initial pressure for a successful transmission is decreased by artificially generating instabilities using small obstacles placed at the tube exit and increased by damping transverse instabilities via porous tube walls, while generating or damping instabilities have minimal effects for weakly unstable mixtures [10,11]. The re-initiation mechanism was also investigated in recent experiments using high-speed flow visualization [12]. The photographs highlight that the mechanism is a consequence of local instabilities within the region between the leading shock and decoupled reaction zone, resulting in an explosion bubble and a new transverse detonation sweeping through the shocked, barely reacted gas. These experimental results thus suggest that cellular instability and transverse waves are important factors for a successful detonation (re-) initiation.

While the aforementioned investigations generally considered a 90° expansion corner, the study of detonation diffraction with various deviation angles θ_w is drawing more attention mainly due to the recent development of detonation-based engines. The shock wave Chester–Chisnell–Whitham (CCW) theory [13] was applied by Bartlmä and Schröder [14] and Thomas et al. [15] to study the shape of diffracted detonation fronts with $\theta_w \geq 30°$. Two different re-initiation mechanisms were found by Thomas et al. [15] and Khasainov et al. [16] for various θ_w. The study of Nagura et al. [17,18] and Kasahara and Kawasaki [19] focused on the transverse detonation in the re-initiation process for large values of θ_w, reporting that both the positions of wall reflection point and local explosion were independent of θ_w and initial pressure p_0. However, the detailed mechanism has not been elucidated by these authors.

Following Nagura's study, a semi-analytical model was constructed in this work to predict the trajectory of the transverse detonation in the re-initiation process of a diffracted cellular detonation wave. Since a highly unstable detonation wave with an irregular cellular pattern may reveal excessive complexity in the diffraction process and has a different re-initiation mechanism from the weakly unstable one, only the weakly unstable detonation wave with regular cellular structure is considered in this work. The paper is organized as follows. In Sect. 2, the problem considered in the simulations is described and the computational details for solving the governing equations are provided. Several characteristics of cellular detonation wave diffraction revealed from the simulation results are reported and discussed in Sect. 3. Using the numerical observations, together with the CCW theory, a semi-analytical model was then constructed. The detailed calculation process and a validation of the model are presented in Sect. 4. In Sect. 5, the model is applied to analyze the re-initiation process, especially to elucidate the mechanisms underlying the experimental results of Nagura et al. Section 6 concludes and highlights the key findings of this work.

2 Numerical method and computational setup

2.1 Numerical method

In the present study, numerical simulations were first performed to reveal some key characteristics of cellular detonation wave diffraction. The numerical results are then used to examine the predictive capability of the proposed semi-analytical model. The adaptive mesh refinement code AMROC [20,21] was adopted to complete the simulations. It is an open-source code based on the structured adaptive mesh refinement (SAMR) technique [22]. The code supports abundant Euler solvers based on TVD and WENO schemes and has been integrated in the virtual test facility (VTF) software. It is widely applied in multi-dimensional detonation simulations [23–28]. In this paper, the two-dimensional reactive Euler equations were used as the governing equations. A second-order accurate shock-capturing MUSCL-TVD finite volume method (FVM) was adopted. The first-order accurate Godunov splitting method was used to handle the reaction source term. A difference scheme with second-order accuracy in space and time was constructed by the Van Albada limiter with MUSCL reconstruction and the Runge–Kutta technique [29], respectively.

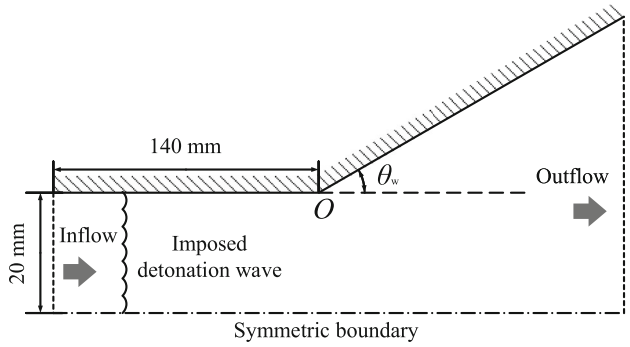

Fig. 1 Schematic of calculation domain: O, expansion corner tip; θ_w, deviation angle

The simulations of cellular detonation wave diffraction were conducted in a two-dimensional computational domain, as shown in Fig. 1. It had a symmetric bottom boundary to display half of the diffraction flow field. The stoichiometric H_2/O_2 mixture with 70% argon dilution under temperature of 298 K was distributed in the domain, and the detailed reaction model of nine species and 34 elementary reactions [30] was employed. To initialize the computation, a self-sustained cellular detonation under the specified initial conditions was first achieved and then imposed near the inlet domain. More details about the initiation procedure were discussed in previous research [23,24]. In the present study, the deviation angle θ_w varied from 10° to 90° in an increment of 10°. In addition, various initial pressures p_0 were chosen to change the cell width λ to satisfy the relation of $D_{inlet} = 13\lambda$, 14λ, 17λ, 20λ, and 25λ, where D_{inlet} represents the full width of the inlet domain (double the inlet domain width shown in Fig. 1), and by preset simulations, the corresponding initial pressures p_0 were 20 kPa, 22 kPa, 25 kPa, 28 kPa, and 32 kPa. According to the re-initiation criterion of $d_c = 13\lambda$ [3], all the simulations are under supercritical condition, which can realize re-initiation successfully. It is worth noting that quantitative cell size comparison between numerical simulations and experimental measurement remains uncertain. Besides the details of numerical methods, such comparison also highly depends on the chemical kinetics model and non-equilibrium effects, especially for H_2/O_2 mixtures [31,32], and hence, to be consistent, all the cell sizes reported in this work are based on the numerical values obtained from the present simulations.

2.2 Grid resolution and time step study

To investigate the effect of grid resolution on the simulations, a series of verification computations for detonation wave diffraction with different mesh refinement strategies were conducted with the conditions of $\theta_w = 90°$ and $p_0 = 22$ kPa. Even under the same grid resolution, different numbers of time steps may lead to unreliable results [33,34]; thus, the selected simulations were also repeated with different numbers of time steps by varying the Courant–Friedrichs–Lewy (CFL) number. In this paper, the trajectory of the transverse detonation and the position where the transverse detonation reflects on the expansion wave are most significant for verifying our model, so the accuracy of these parameters should be insured primarily. Figure 2 presents the numerical soot foils for three different resolutions, where $l_{ig}/\Delta x_{min}$ represents the number of grid points per induction length in the highest refinement area, and Fig. 3 shows the trajectories of the transverse detonation for different resolutions and CFL numbers. The distance L_w from the wall reflection point to the expansion corner tip for each resolution and CFL number is listed in Table 1. It can be observed that the trajectory is not very sensitive to the chosen grid resolutions and CFL numbers, and the distance L_w of all cases is essentially the same. Considering the computational cost, the resolution of $l_{ig}/\Delta x_{min} = 16$ and the CFL number of 0.95 were applied for all the following simulations.

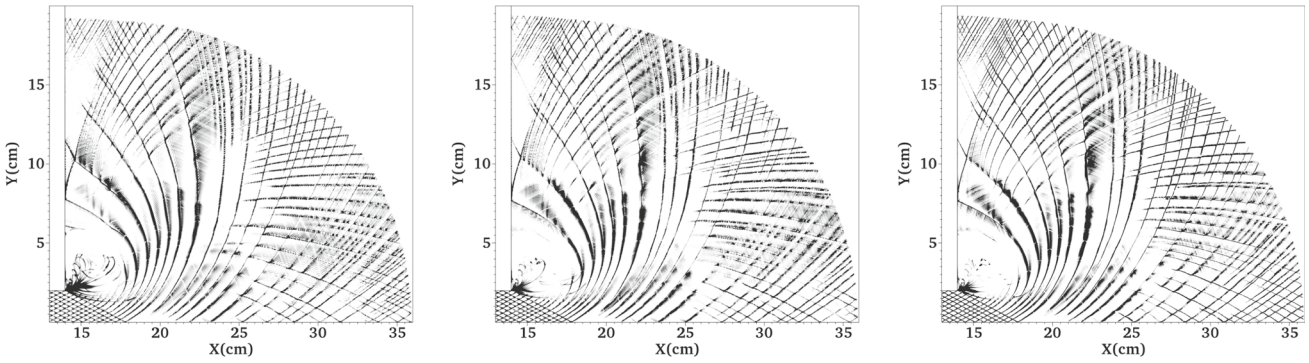

(a) $l_{ig}/\Delta x_{min} = 8, \mathrm{CFL} = 0.95$ **(b)** $l_{ig}/\Delta x_{min} = 16, \mathrm{CFL} = 0.95$ **(c)** $l_{ig}/\Delta x_{min} = 32, \mathrm{CFL} = 0.95$

Fig. 2 Numerical soot foils of detonation wave diffraction for three different mesh resolutions

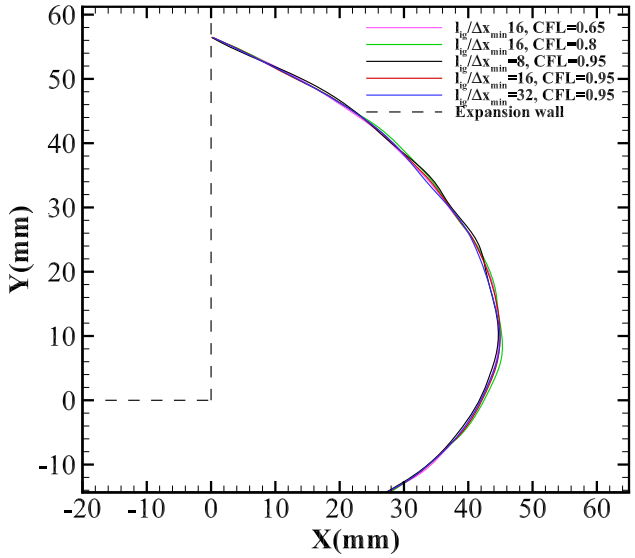

Fig. 3 Trajectories of transverse detonation for different mesh resolutions and CFL numbers

Table 1 Wall reflection point distance L_w for different mesh resolutions and CFL numbers

Condition	L_w (mm)
$l_{ig}/\Delta x_{min} = 16$, CFL $= 0.65$	56.469
$l_{ig}/\Delta x_{min} = 16$, CFL $= 0.8$	56.483
$l_{ig}/\Delta x_{min} = 8$, CFL $= 0.95$	56.462
$l_{ig}/\Delta x_{min} = 16$, CFL $= 0.95$	56.478
$l_{ig}/\Delta x_{min} = 32$, CFL $= 0.95$	56.448

3 Numerical observations of cellular detonation diffraction

Before starting to build the model, results from numerical simulations were explored. Three key characteristics for the weakly unstable detonation diffraction were determined, which are the essence of the present model development.

3.1 The initial position of the transverse detonation

The position where local explosion occurs in the re-initiation process, i.e., the initial location of the transverse detonation, was first studied theoretically by Edwards et al. [2]. These authors reported that the location of local explosion was on the expansion wave front with a horizontal distance of $s_t = 5\lambda \cot\alpha$ to the channel exit, where λ and α represent the cell width and the horizontal angle of the expansion wave front, respectively, as shown in Fig. 4. However, recent studies [8,18] claimed that the position of local explosion is related to the deviation angle θ_w, instead of on the expansion wave front. Figures 5 and 6 display the numerical soot foils and the enlarged views with overlay of density-gradient

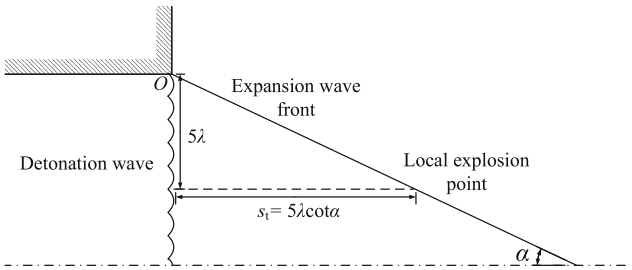

Fig. 4 Sketch of position where local explosion occurs in Edwards's theory: s_t, horizontal distance from position of local explosion to channel exit; α, horizontal angle of expansion wave front; λ, detonation cell width

schlieren and cellular pattern presenting the re-initiation process for various θ_w. The newly generated detonation cells at the position of $x > 30$ cm in the soot foils, which have the approximate size with the original ones, indicate that the detonation re-initiation process has completed. These results show that when $\theta_w < 30°$, the transverse waves reflect on the expansion wall immediately after the detonation wave propagates into the expansion area, which leads to a local explosion in the vicinity of the wall, and the detonation wave can propagate sustainably without decoupling, as shown in Fig. 5. While $\theta_w \geq 30°$, the detonation wave front near the wall decouples first, then a local explosion occurs, and a transverse detonation is generated on the upper side of the expansion cone, as shown in Fig. 6. Since this case corresponds to a supercritical condition, part of the diffracted detonation does not fail completely by the expansion waves from the corner and near the axis, transverse waves persist, but cells are growing along the diffracted front. It is worth mentioning that this case also corresponds to a weakly unstable detonation and the failure of the diffracted detonation is argued to be caused by an excessive front curvature [9]. Thus, for a supercritical case, the detonation front would not be decoupled near the channel axis since the front curvature there is sufficiently small. These results agree well with the experimental studies of Khasainov et al. [16] and Nagura et al. [18], but the location of the explosion is often unpredictable. Nevertheless, as Fig. 6 shows, it is found that the transverse detonation stems from a location on the expansion wave front. Although one cannot determine the exact coordinates of the local explosion, this initial location can be identified in the numerical soot foil by tracking the trajectory of the transverse detonation (along the red arrow in Fig. 6) back to the expansion wave front. Hence, the horizontal distance s_t from the initial location to the channel exit can be determined. Figure 7 presents the dimensionless value $s_t/\lambda \cot\alpha$ for each case, which represents the contained detonation cell number in the width between the initial location and the channel wall. Since the initial location on the expansion wave front just corresponds to the tip of the detonation cell in the soot foil,

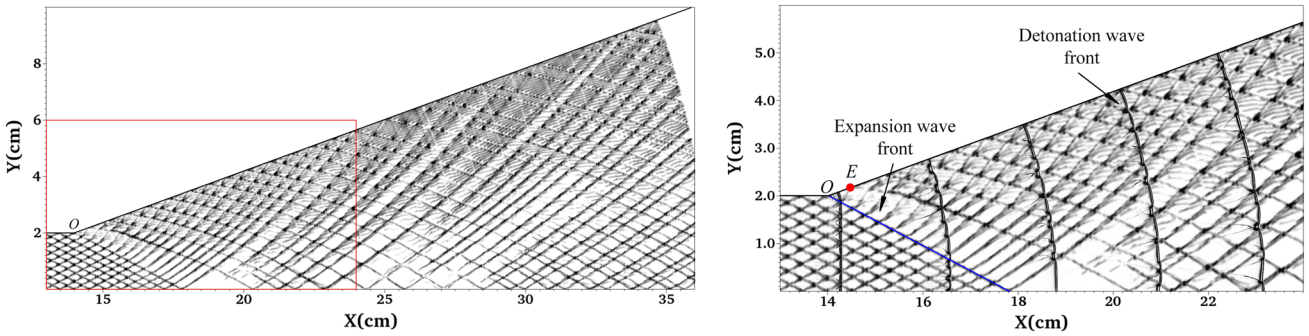

Fig. 5 Numerical soot foil and the enlarged view presenting the re-initiation process of the diffracted detonation wave with $\theta_w = 20°$ and $p_0 = 22$ kPa: E, position of local explosion

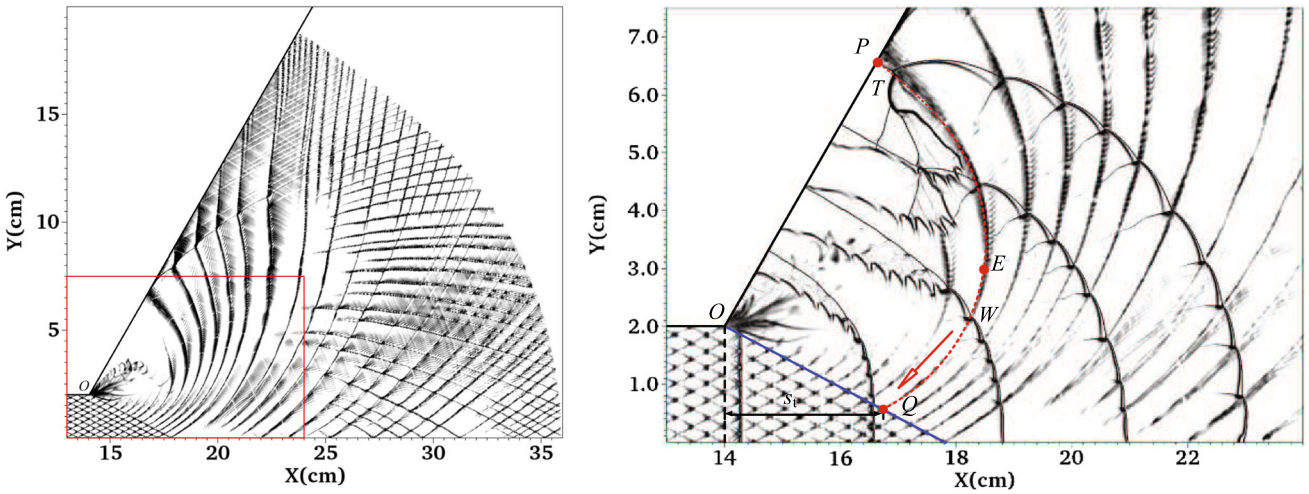

Fig. 6 Numerical soot foil and the enlarged view presenting the re-initiation process of the diffracted detonation wave with $\theta_w = 60°$ and $p_0 = 22$ kPa: P, position of wall reflection point; T, transverse detonation; E, position of local explosion; W, transverse wave; Q, initial location of transverse detonation; s_t, horizontal distance from initial location to channel exit; dotted line represents the trajectory of the transverse detonation

the value $s_t/\lambda \cot\alpha$ must be an integer multiple of 0.5. One can notice that for all the cases, the value $s_t/\lambda \cot\alpha$ increases with θ_w as $\theta_w < 60°$, whereas at $\theta_w \geq 60°$, the value stabilizes at 5, which corresponds to that given in Edwards et al. [2]. Therefore, for the cases with $\theta_w \geq 60°$, the expression from Edwards et al. can be applied to predict the initial location of the transverse detonation on the expansion wave front, i.e., $s_t = 5\lambda \cot\alpha$. Thus, for the cases with $\theta_w \geq 60°$, the initial position of the transverse detonation can be theoretically predicted and used as an input parameter for the semi-analytical model to calculate the subsequent trajectory of the transverse detonation.

3.2 The velocity of the transverse detonation

The velocity of the transverse detonation D_t is another important parameter in our model. The value of the velocity D_t was extracted at each simulation time. Figure 8 shows the relation between dimensionless value D_t/D_{CJ} and simulation time for various initial pressures p_0 with $\theta_w = 90°$. Table 2 lists the total average value of D_t/D_{CJ} for these cases, where D_{CJ} represents the velocity value of a Chapman–Jouguet (CJ) detonation wave under the same condition. The results indicate that the velocity D_t just varies in a small range from $0.94D_{CJ}$ to $1.05D_{CJ}$, and the average velocity is close to D_{CJ} for each case. Therefore, it is reasonable to set D_{CJ} as the velocity value of the transverse detonation in the model calculation, whereas the effect of the deviation will be discussed in Sect. 5. Furthermore, the direction of velocity D_t is another key element to be considered. Figure 9 presents the propagation of the transverse detonation in the re-initiation process. The velocity of the transverse detonation D_t can be considered as a combination of two velocity components: the relative velocity of the transverse detonation to the diffracted detonation wave front D_h and the expansion velocity of the diffracted wave front D_v, as shown in Fig. 9. Since the trans-

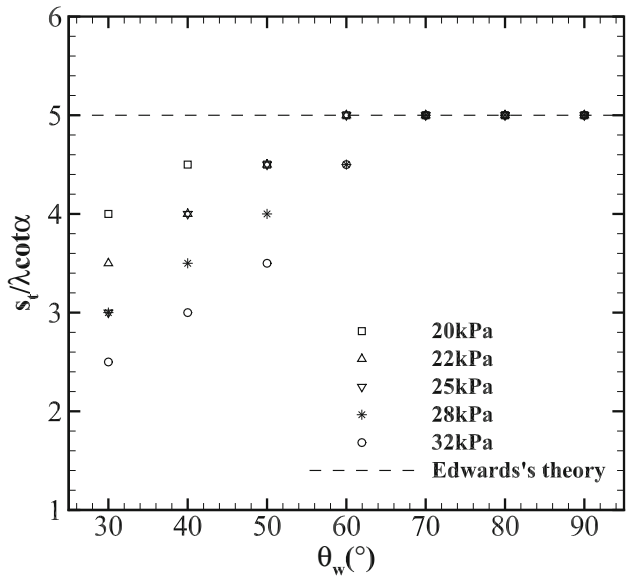

Fig. 7 $s_t/\lambda\cot\alpha$–θ_w relation for various p_0 compared with the Edwards's theory

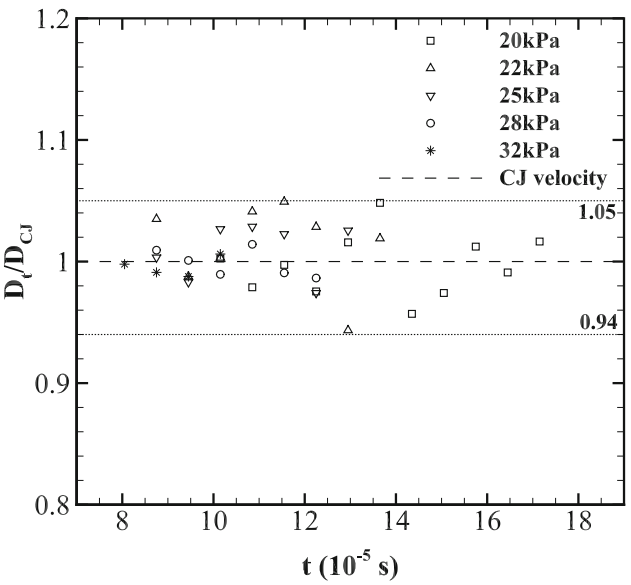

Fig. 8 Relation between dimensionless velocity D_t/D_{CJ} and simulation time for various p_0 with $\theta_w = 90°$

verse detonation always propagates along the diffracted wave front, the velocity D_h should be tangent to the wave front surface, whereas the velocity D_v is perpendicular to the surface, which means D_h and D_v are orthogonal.

3.3 The shape of diffracted detonation wave front

In the present study, the shape of the diffracted detonation wave front was analyzed by comparing with the results of the CCW theory. This theory was first proposed in Whitham's research [13] by adopting the analysis of Chester [35] and

Table 2 Average value of D_t/D_{CJ} for various p_0 with $\theta_w = 90°$

Initial pressure p_0 (kPa)	Average value of D_t/D_{CJ}
20	0.997
22	1.013
25	1.009
28	0.998
32	0.996

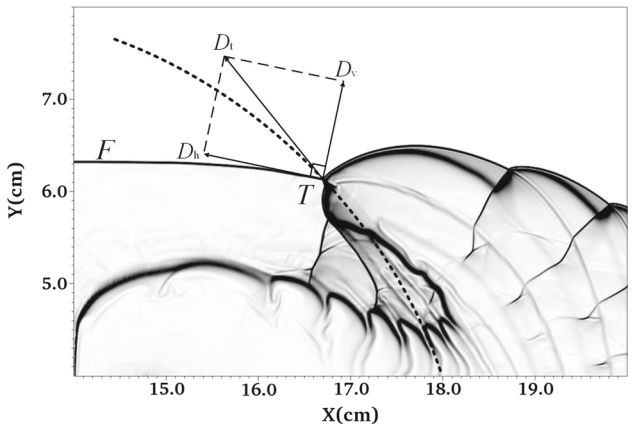

Fig. 9 Sketch showing the separation of the transverse detonation velocity: D_t, velocity of the transverse detonation; D_h, relative velocity of the transverse detonation to diffracted wave front; D_v, expansion velocity of diffracted wave front; T, transverse detonation; F, diffracted detonation wave front; dotted line represents the trajectory of the transverse detonation

Chisnell [36] and then extended by Skews [37] to predict the shape as well as velocity of the diffracted shock wave front with reasonable accuracy. To verify again the accuracy of the theory, a simulation of shock wave diffraction was conducted under the Mach number $M_s = 4.7$ and $\theta_w = 90°$. The shape of the diffracted shock wave front was compared with the results calculated by the CCW model (the detailed calculation process of the model will be introduced in Sect. 4), as presented in Fig. 10. It can be observed that the results of the CCW model agree well with the shape of the shock front.

As to detonation wave diffraction, it is known that the flow state behind the wave front is highly non-uniform, which is different from the inert shock wave, so theoretically the CCW model cannot be applied directly to predict the shape of the diffracted detonation wave. It is worth noting that in recent years, a number of remedies have been proposed by several researchers to address the effect of flow non-uniformity [38–41], for example, by coupling the post-shock flow conditions obtained from simulations or existing data into the zero-order leading shock front solution. Nevertheless, for simplicity, the original CCW formulation is retained in the present study to illustrate the proposed modeling strategy. Furthermore, as introduced in Sect. 3.1, the detonation wave front will decouple in the diffraction process for $\theta_w \geq 30°$,

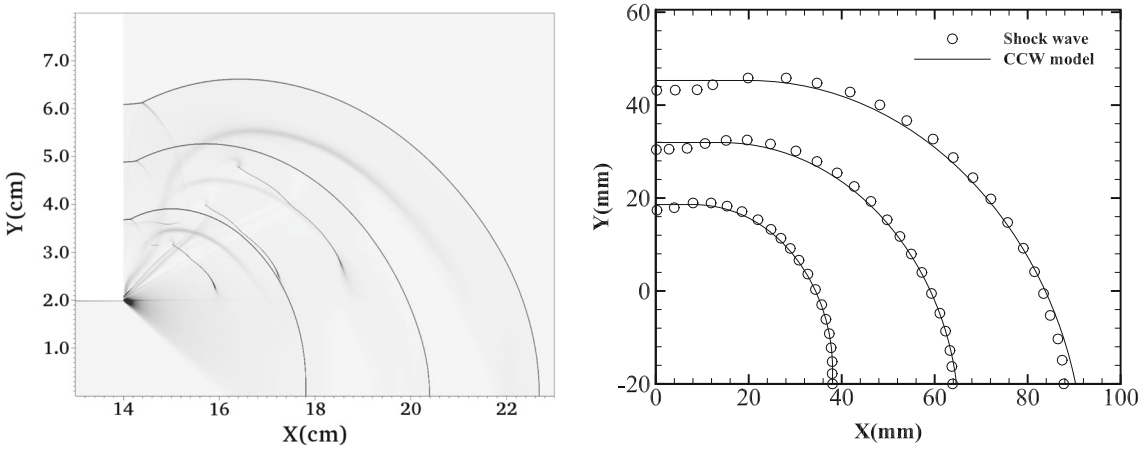

Fig. 10 Density-gradient schlieren of diffracted shock wave front and corresponding coordinates compared with the CCW model results at different simulation times ($M_s = 4.7$, $\theta_w = 90°$)

and the decoupled detonation wave has similar flow structure with shock wave. Bartlmä and Schröder [14] showed that the shape of the decoupled wave front is the same as that of a diffracted inert shock wave front under the same Mach number, which implies that the shape of the decoupled region of the diffracted detonation wave front is self-similar and could be predicted by the CCW model for a diffracted shock wave. However, as to the diffraction of detonation wave, local explosion and re-initiation will be generated in supercritical condition, which is beyond the consideration of the study of Bartlmä and Schröder. To describe the shape of detonation wave after re-initiation, the density-gradient schlieren of diffracted detonation waves at different times were captured and overlaid for various cases, as shown in Fig. 11a, c, e. It can be clearly seen that the local explosion happens and a transversely propagating detonation wave is generated, dividing the decoupled wave front from the coupled detonation wave. Simultaneously, the center coupled detonation wave spreads with a convex front, whereas the decoupled portion of the wave with smooth front is swept by the transverse detonation and finally disappears as the transverse detonation reaches the expansion wall and reflects. The symbols plotted in Fig. 11b, d, f indicate the coordinates extracted from the diffracted detonation wave fronts shown in Fig. 11a, c, e and are compared with the corresponding results calculated by the CCW model for inert shock diffraction (plotted as black curves). As shown in the first and second sets of curves in Fig. 11b, d, f, the shape of the decoupled wave front (plotted as circular symbols) is coincident with the theoretical curve under the condition of various θ_w and p_0 at different times, while the shape of the coupled detonation wave front (plotted as triangular symbols) deviates from the theoretical curve gradually due to its different flow states behind the wave front comparing with shock wave. Moreover, when the transverse detonation reflects on the expansion wall, the entire wave front becomes coupled, thus making the shape of the entire wave front no longer coincide with the theoretical result, as shown in the third set of curves in Fig. 11b, d, f. Consequently, it is confirmed that in the re-initiation process of detonation wave diffraction, although the shape of the coupled detonation wave front with non-uniform flow state is totally different from the prediction by the CCW model, the shape of the decoupled wave front, which can be regarded as a shock wave, agrees well with the theoretical result despite the effect of the local explosion and thus can be predicted accurately by the CCW theory. It must be emphasized that despite such good agreement for the present validation case in Fig. 10 and comparison shown in Fig.11 for the decoupled part of the diverging detonation, the CCW theory remains a zero-order approximate model considered in this work as it does not retain all flow characteristics behind the leading shock in the original formulation. In fact, the use of the CCW theory in the present model can be relaxed and will be considered in the future by incorporating more recent geometrical shock waves models, e.g., [42], to describe the propagation of the decoupled detonation required in this work.

4 The semi-analytical model setup

With the key characteristics of weakly unstable detonation diffraction being investigated numerically, the semi-analytical model to predict the trajectory of the transverse detonation can now be built. The calculation process and the verification of the model are presented in detail here.

4.1 The CCW model for diffracted detonation wave

Since the CCW theory neglects the influence of the flow field behind the wave front, it is more accurate for large deviation

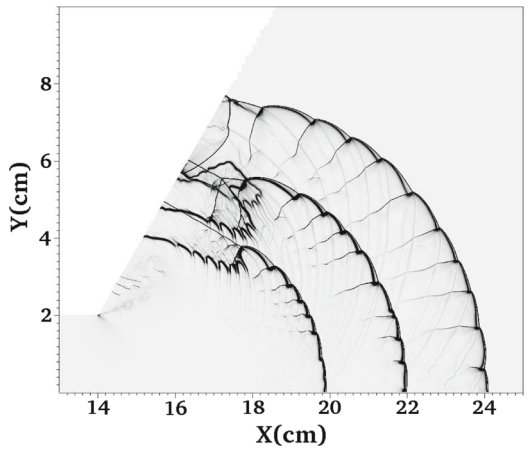

(a) $\theta_w = 60^\circ$ and $p_0 = 22$ kPa.

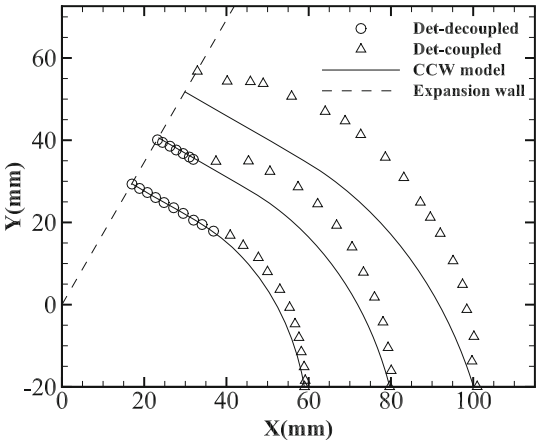

(b) $\theta_w = 60^\circ$ and $p_0 = 22$ kPa.

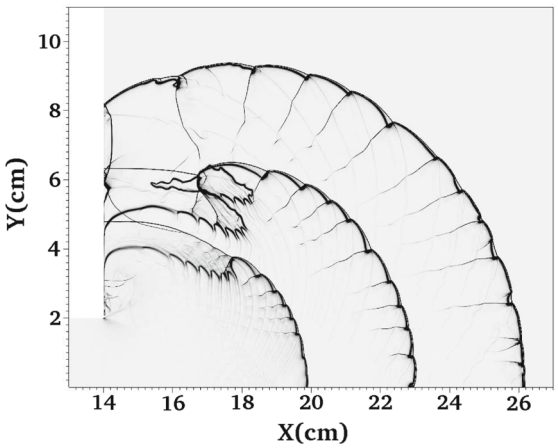

(c) $\theta_w = 90^\circ$ and $p_0 = 22$ kPa.

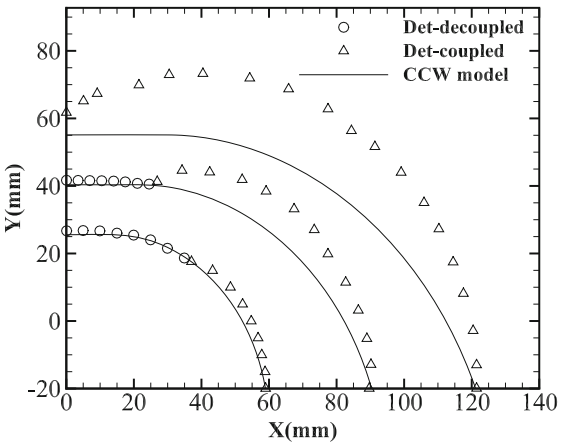

(d) $\theta_w = 90^\circ$ and $p_0 = 22$ kPa.

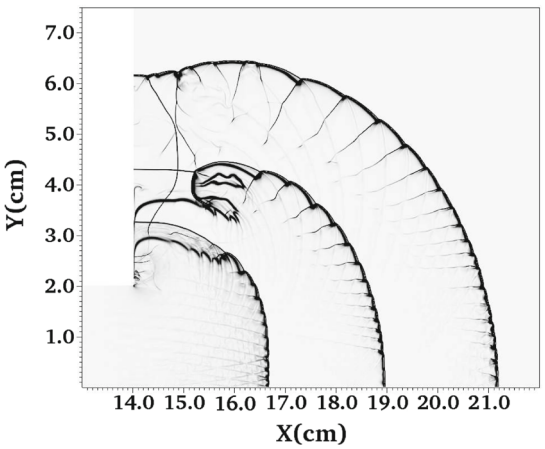

(e) $\theta_w = 90^\circ$ and $p_0 = 32$ kPa.

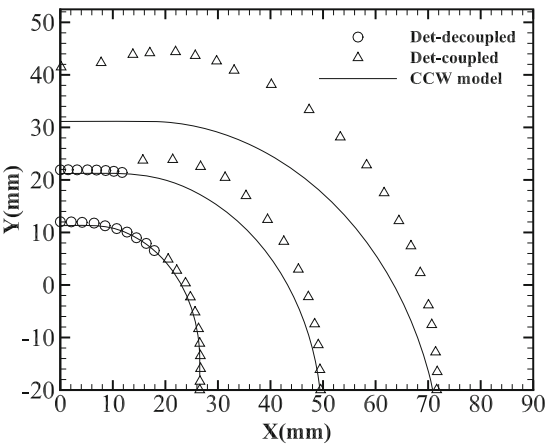

(f) $\theta_w = 90^\circ$ and $p_0 = 32$ kPa.

Fig. 11 Density-gradient schlieren of diffracted detonation wave front and corresponding coordinates compared with the CCW model results for various θ_w and p_0 at different simulation times

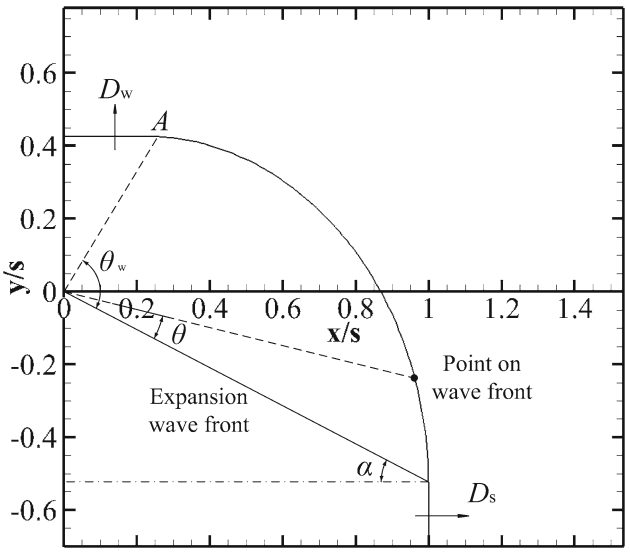

Fig. 12 Theoretical dimensionless shape of diffracted shock wave with $\theta_w = 90°$ and $\gamma = 1.4$: D_w, velocity of wave front near expansion wall; D_s, velocity of unaffected shock wave; θ, center angle from expansion wave front to a certain point on diffracted shock front; A, end of curved wave front

angles and strong shock waves ($M^2 \gg 1$) [43–45]. As to the diffracted shock wave, the CCW model yields convenient results in a closed analytical form. The shape of the diffracted shock wave can be given by:

$$\left.\begin{aligned} x/s &= \left(\sqrt{n+1}/\sqrt{n}\right) \mathrm{e}^{-\theta/\sqrt{n}} \cos(\alpha-\theta) \\ y/s &= -\left(\sqrt{n+1}/\sqrt{n}\right) \mathrm{e}^{-\theta/\sqrt{n}} \sin(\alpha-\theta) \end{aligned}\right\} 0 \le \theta \le \theta_w, \tag{1}$$

where x and y represent the coordinates of point on the diffracted shock wave front, s the horizontal distance from channel exit to the unaffected shock wave, and θ the angle from expansion wave front to the corresponding point. Moreover, for strong shock waves, the parameters n and α can be obtained approximately by:

$$n = (\gamma+2)/\gamma + \sqrt{2\gamma/(\gamma+1)} \quad \text{and} \quad \tan^2\alpha = 1/n, \tag{2}$$

where γ is the specific heat ratio. The dimensionless shape of diffracted shock wave calculated by (1) with $\theta_w = 90°$ and $\gamma = 1.4$ is shown in Fig. 12. It can be found that the shape is self-similar and determined by s. It is also noticed that the wave front after point A is straight and perpendicular to the wall.

As claimed in Sect. 3.3, the CCW theory can be applied to predict the shape of the decoupled wave front. As the terminal point of the decoupled wave front, the coordinates of the transverse detonation also satisfy the relation in (1). Thus, once we obtain the angle θ where the transverse detonation locates and the horizontal distance s of the corresponding

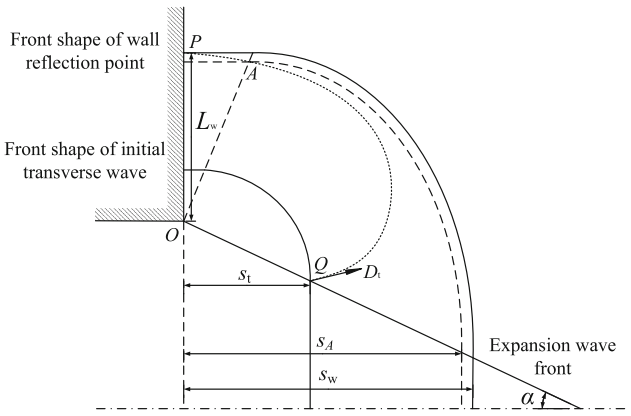

Fig. 13 Sketch of the transverse detonation trajectory: P, position of wall reflection point; A, end of curved wave front; Q, initial location of transverse detonation; L_w, distance from wall reflection point to expansion corner tip; s_t, horizontal distance of initial location; s_A, horizontal distance of wave front with point A on it; s_w, horizontal distance of wave front when the transverse detonation reaches expansion wall; dotted line represents the trajectory of the transverse detonation

wave front for the entire re-initiation process, the trajectory as well as the wall reflection position can be calculated by (1).

The expansion velocity of the decoupled wave front can also be calculated by the CCW model. Considering that the velocity of the unaffected detonation wave equals D_{CJ}, the velocity of the straight wave front perpendicular to the wall D_w can be given by:

$$D_w = D_{CJ}\mathrm{e}^{\theta_w/\sqrt{n}}. \tag{3}$$

From (1), it is realized that the wave front shape in the range from 0 to θ_w can always be coincident as θ_w changes, and the velocity D_w is always perpendicular to the wave front. Thus, we can approximate the expansion velocity D_v of any point on the decoupled wave front as:

$$D_v = D_{CJ}\mathrm{e}^{\theta/\sqrt{n}}. \tag{4}$$

4.2 Calculation process

The sketch of the transverse detonation trajectory is shown in Fig. 13. To predict the full trajectory, we should obtain the angle θ of the transverse detonation and the distance s of the corresponding wave front at each time. As mentioned in Sect. 3.1, theoretically the calculation should start at the initial location on the expansion wave front Q with the coordinates of $x_0 = s_t = 5\lambda\cot\alpha$ and $y_0 = -5\lambda$. However, the velocity D_t at point Q is perpendicular to the wave front, which means the velocity component $D_{h0} = 0$ and the calculation cannot continue at the beginning. To avoid this situation, a certain point which is extremely close to the point

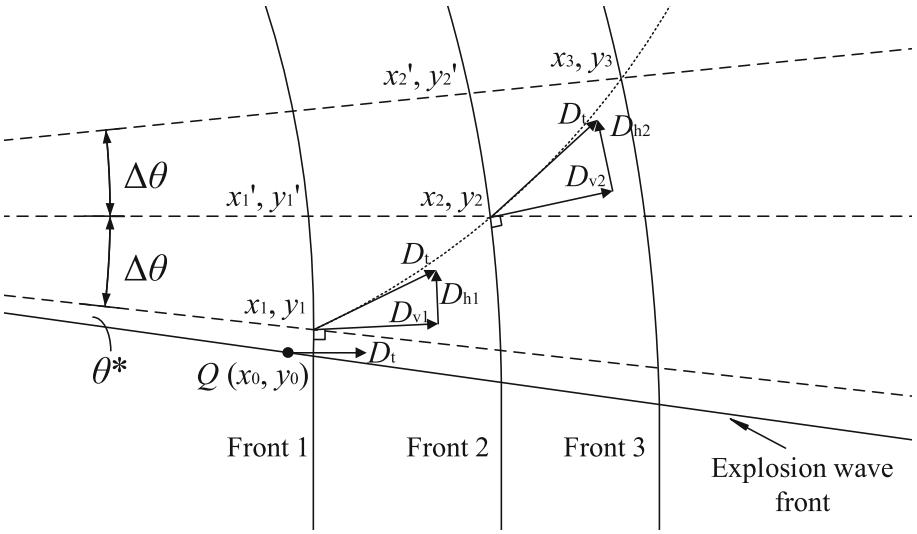

Fig. 14 Sketch of the first step in the calculation process of model: dotted line represents the trajectory of the transverse detonation

Q with the coordinates of $x_1 = x_0 + l^*$ and $y_1 = y_0 + l^*$ is chosen as the initial point, where l^* represents an extremely short preset distance set equal to 0.05 mm in the present calculation. The area around the point (x_1, y_1) as well as the initial calculation step is displayed schematically in Fig. 14. The angle θ^* from the expansion wave front to point (x_1, y_1) can be obtained easily by:

$$\theta^* = \alpha - \arctan\left|y_1/x_1\right|. \tag{5}$$

So the distance s_1 from the channel exit to the unaffected wave front in Front 1 can be calculated by (1):

$$s_1 = x_1/\left(\left(\sqrt{n+1}/\sqrt{n}\right)\mathrm{e}^{-\theta^*/\sqrt{n}}\cos(\alpha-\theta^*)\right) \approx s_t. \tag{6}$$

As discussed in Sect. 3.2, it is assumed that the velocity of the transverse detonation is $D_t = D_{CJ}$ and the velocity components D_h and D_v are orthogonal. According to (4), the components D_{v1} and D_{h1} at point (x_1, y_1) can be expressed as:

$$D_{v1} = D_{CJ}\mathrm{e}^{\theta^*/\sqrt{n}}, \tag{7}$$

$$D_{h1} = D_{CJ}\sqrt{1-\left(\mathrm{e}^{\theta^*/\sqrt{n}}\right)^2}. \tag{8}$$

As shown in Fig. 14, assuming that the transverse detonation moves from (x_1, y_1) to (x_2, y_2), with a known small angle variation of $\Delta\theta$ (e.g., $\Delta\theta = 1°$, the coordinates of point (x_2, y_2) are still unknown), then the coordinates of the corresponding point (x_1', y_1') with the same angle variation $\Delta\theta$ on Front 1 can be obtained by:

$$\begin{aligned} x'_1 &= s_1\left(\sqrt{n+1}/\sqrt{n}\right)\mathrm{e}^{-(\theta^*+\Delta\theta)/\sqrt{n}}\cos\left(\alpha-(\theta^*+\Delta\theta)\right), \\ y'_1 &= -s_1\left(\sqrt{n+1}/\sqrt{n}\right)\mathrm{e}^{-(\theta^*+\Delta\theta)/\sqrt{n}}\sin\left(\alpha-(\theta^*+\Delta\theta)\right). \end{aligned} \tag{9}$$

Therefore, the time Δt_1 when the transverse detonation moves from (x_1, y_1) to (x_2, y_2) can be calculated approximately by:

$$\Delta t_1 = \Delta l_1/D_{h1} \approx \sqrt{(x'_1 - x_1)^2 + (y'_1 - y_1)^2}/D_{h1}. \tag{10}$$

Then, the horizontal distance s_2 for Front 2 can be determined by:

$$s_2 = s_1 + D_{CJ}\Delta t_1, \tag{11}$$

and the coordinates of point (x_2, y_2) can be confirmed by:

$$\begin{aligned} x_2 &= s_2\left(\sqrt{n+1}/\sqrt{n}\right)\mathrm{e}^{-(\theta^*+\Delta\theta)/\sqrt{n}}\cos\left(\alpha-(\theta^*+\Delta\theta)\right), \\ y_2 &= -s_2\left(\sqrt{n+1}/\sqrt{n}\right)\mathrm{e}^{-(\theta^*+\Delta\theta)/\sqrt{n}}\sin\left(\alpha-(\theta^*+\Delta\theta)\right). \end{aligned} \tag{12}$$

This completes the first step of the calculation. After repeating the calculations from (9) to (12) for the counts of $n = \theta_w/\Delta\theta$, the transverse detonation will finally reach the end of the curved wave front A in Fig. 13, and the trajectory of the transverse detonation from point Q to point A can be confirmed by tracking its location in each step. The coordinates of point A as well as the horizontal distance s_A can be obtained by the last step of the calculation.

The trajectory after point A should also be considered. The area around point A is presented in Fig. 15. It has been pointed out that the wave front behind the point A is straight and perpendicular to the wall with a constant velocity of $D_{vw} = D_{CJ}\mathrm{e}^{\theta_w/\sqrt{n}}$, so the component velocity D_{hw} of the transverse detonation is also constant at:

$$D_{hw} = D_{CJ}\sqrt{1-\left(\mathrm{e}^{\theta_w/\sqrt{n}}\right)^2}. \tag{13}$$

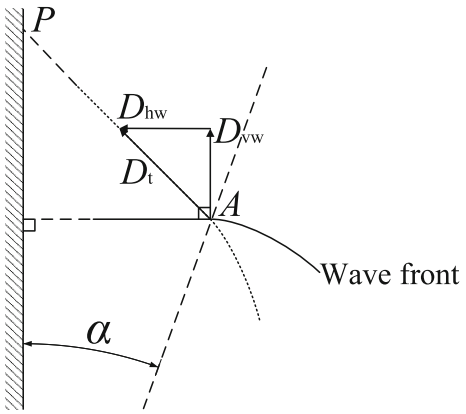

Fig. 15 Sketch of trajectory behind point A: dotted line represents the trajectory of the transverse detonation

It can be inferred that this part of trajectory is also straight. Since the coordinates of point A have been known as (x_A, y_A), the vertical distance L_v from point A to the channel wall can be calculated by:

$$L_v = \sqrt{x_A^2 + y_A^2}\sin\alpha. \tag{14}$$

Thus, the time t_w when the transverse detonation moves from point A to the wall can be given by:

$$t_w = L_v / D_{hw}, \tag{15}$$

and the horizontal distance s_w when the transverse detonation reaches the wall is known as:

$$s_w = s_A + D_{CJ} t_w. \tag{16}$$

According to (1), the distance of wall reflection point L_w can be obtained by:

$$L_w = s_w \left(\sqrt{n+1}/\sqrt{n}\right) e^{-\theta_w/\sqrt{n}} \cos\alpha. \tag{17}$$

It is clear that the trajectory after point A is a straight line connecting point A and the wall reflection point; thus, the entire trajectory of the transverse detonation is established. In the present work, the calculation process is realized by MATLAB®, and the flow parameters are calculated by CANTERA.

4.3 Validation of the model

It is realized that in the calculation process, the parameter $\Delta\theta$ can be regarded as the resolution of the model, so the effect of various $\Delta\theta$ on the calculated results should be investigated. The $\Delta\theta$ of 2°, 1°, 0.5°, 0.25°, and 0.125° were chosen to calculate the same condition of $p_0 = 22$ kPa and $\theta_w = 90°$; the trajectories calculated by the present model with various $\Delta\theta$ are shown in Fig. 16. It can be visualized that the curves are close to each other with only a slight deviation among them. This indicates that all the above increments $\Delta\theta$ can be applied in the model with certain precision. Here, the resolution of $\Delta\theta = 0.5°$ is adopted in the present analysis. Moreover, in order to verify the accuracy of the model, several comparisons between the transverse detonation trajectories in simulations and the corresponding results calculated by the model were conducted with various θ_w and p_0, as displayed in Fig. 17. In addition, the wall reflection point distance L_w for each simulation case and model prediction is presented in Fig. 18. It should be noted that the trajectories and reflection points for simulations are all extracted from the numerical soot foil. Due to the limited resolution, the extraction has a certain error, which is presented as error bars in the figures. Additionally, since the range of θ_w we simulated is from 10° to 90°, only the results for cases with $90° \geq \theta_w \geq 60°$ can be compared with the results of model, whereas the model can extend easily to a wider range of θ_w, as Fig. 18 shows. From the figures, all the trajectory curves as well as the distances L_w calculated by model are in good agreement with the simulation results, which indicates that the model can predict the trajectory of the transverse detonation accurately under the limitation of $\theta_w \geq 60°$.

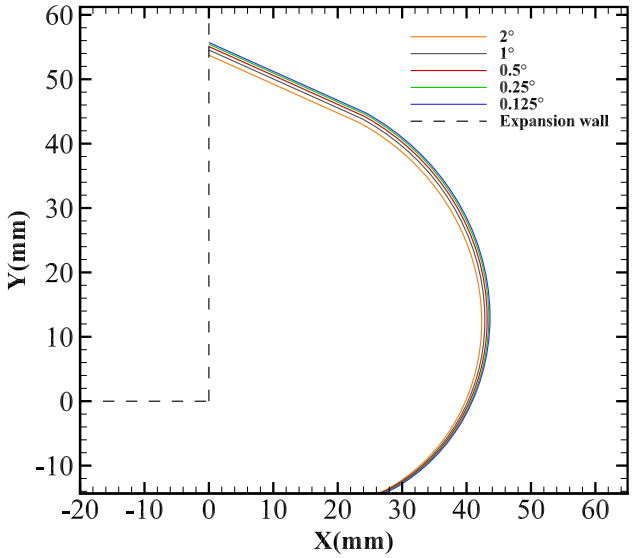

Fig. 16 Trajectories of the transverse detonation calculated by model for various $\Delta\theta$ under $p_0 = 22$ kPa and $\theta_w = 90°$

5 Analysis of the model

Since the predictive capability of the model has been verified, the model can be applied to revisit the characteristics of the transverse detonation in the re-initiation process. As intro-

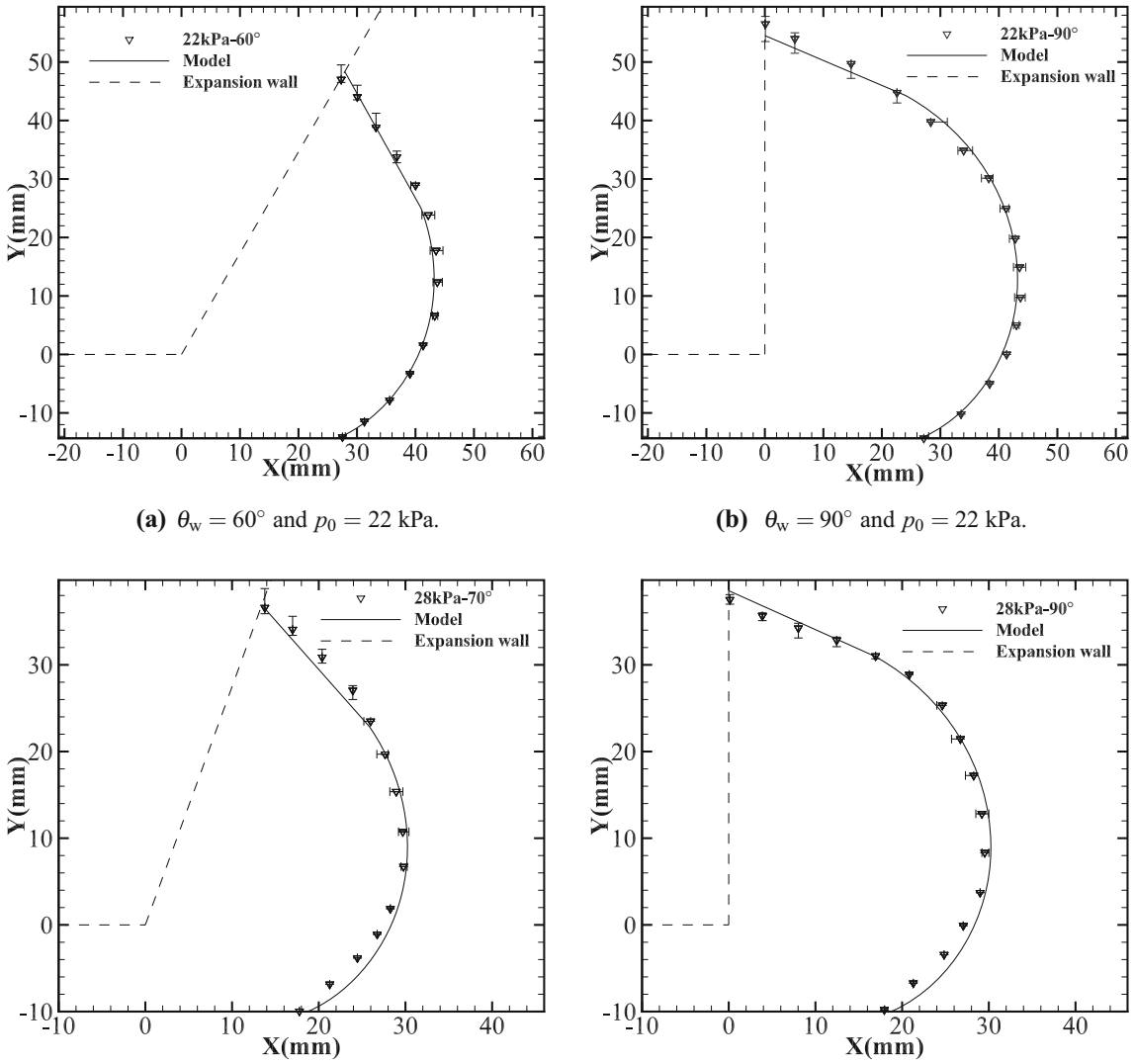

(a) $\theta_w = 60°$ and $p_0 = 22$ kPa.

(b) $\theta_w = 90°$ and $p_0 = 22$ kPa.

(c) $\theta_w = 70°$ and $p_0 = 28$ kPa.

(d) θ_w=90° and $p_0 = 28$ kPa.

Fig. 17 Comparison of trajectories for simulation and model with various θ_w and p_0

duced in Sect. 1, in Nagura's research [17,18], an important conclusion was drawn that for $150° \geq \theta_w \geq 60°$, independent of θ_w and p_0, the distance L_w varies in a small range of $(12.3 \pm 4.1)\lambda$ in experimental observation, and the range increases to about 20λ in two-dimensional simulations, but the mechanism of this observation has not been given. By applying the present model, the underlying mechanism can be explained. Figures 18 and 19 show the L_w–θ_w and L_w/λ–θ_w relation calculated by the model for various p_0 with $150° \geq \theta_w \geq 60°$, respectively. It can be seen clearly from Fig. 18 that the value of L_w decreases with increasing p_0. Nevertheless, at $90° \geq \theta_w \geq 60°$, the L_w appears almost unchanged and just decreases slowly along with θ_w when $\theta_w > 90°$. It is also found from Fig. 19 that the L_w/λ–θ_w curves are perfectly coincident at a common model curve for various p_0, and the value of L_w/λ varies between 15 and 20, so strictly speaking the distance L_w still has relation with θ_w, but the deviation against θ_w is minimal and may be hard to distinguish in experiments. Since the model is inferred by the three features of cellular detonation wave diffraction discussed in Sect. 3, we can deduce that this trend of nearly stable value of the distance L_w against θ_w is just a natural result determined by those three characteristics.

As to that the parameter L_w/λ is constant for the same θ_w and independent of p_0, it is noticed from (6) to (12) that the parameters x_1', y_1', Δt_1, s_2, x_2, and y_2 can all be expressed by a form of s_1 multiplied by a function of $\Delta\theta$ since the parameters n, θ^*, θ_w, and α can be seen as constant for various p_0. In addition, we have known that s_1 is an approximate parameter of s_t, so it can be inferred that the trajectory of the transverse detonation can be re-expressed in a dimensionless form:

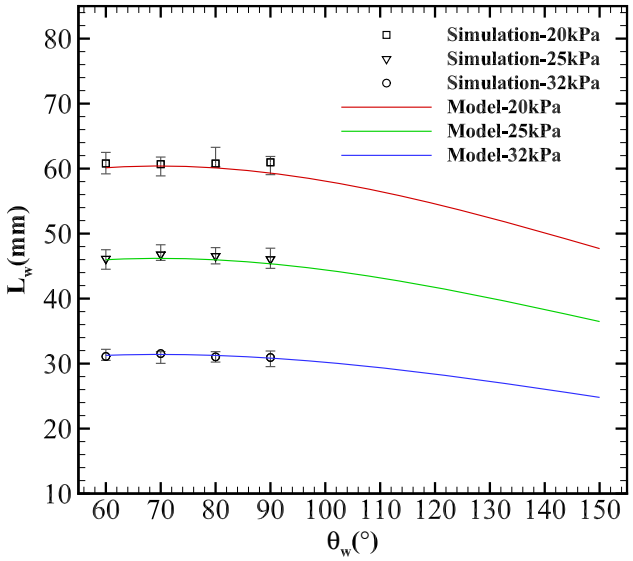

Fig. 18 Comparison of distance of wall reflection point L_w for simulation and model with various θ_w and p_0

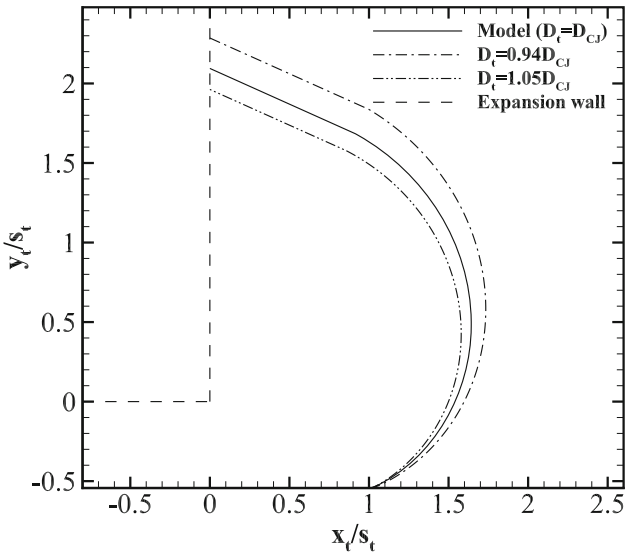

Fig. 20 Dimensionless trajectories of the transverse detonation for various p_0 and D_t with $\theta_w = 90°$ (curves for various p_0 are coincident)

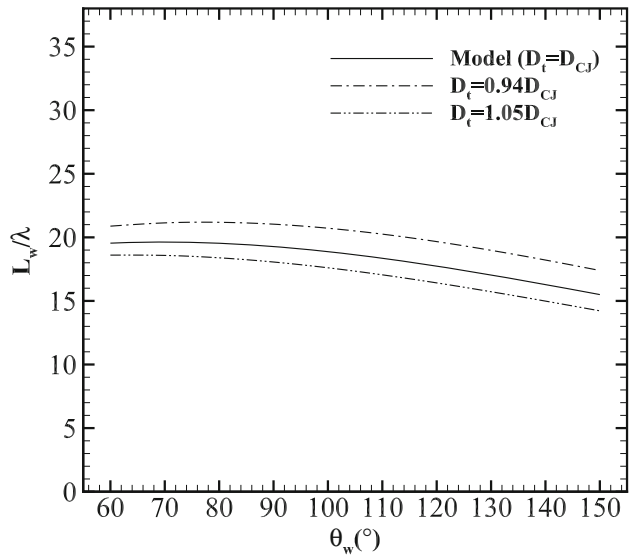

Fig. 19 L_w/λ–θ_w relation calculated by model for various p_0, θ_w, and D_t (curves for various p_0 are coincident)

$$\begin{aligned} x_t/s_t &= f\,(\Delta\theta)\,, \\ y_t/s_t &= g\,(\Delta\theta)\,, \end{aligned} \tag{18}$$

where x_t and y_t represent the coordinates of point on the trajectory. The dimensionless trajectories with $\theta_w = 90°$ are shown in Fig. 20. Similar to Fig. 12, the trajectories are also found to be self-similar and only related to the distance s_t, which leads to the dimensionless trajectories coincident at one model curve for various p_0. Thus, the relation of $s_t = 5\lambda \cot \alpha$ determines that the parameter L_w/λ can be regarded as constant for the same θ_w and independent of p_0. It is also implied that this characteristic is available for all the weakly unstable detonation waves with constant cell width.

As mentioned in Sect. 3.2, the velocity D_t does not exactly equal D_{CJ}, which varies in a range between $0.94D_{CJ}$ and $1.05D_{CJ}$. To discuss the effect of the deviation on the trajectory calculated by the model, the dimensionless value L_w/λ and trajectories for $D_t = 0.94D_{CJ}$ and $D_t = 1.05D_{CJ}$ are presented in Figs. 19 and 20, respectively. It is found from Fig. 20 that as D_t changes, the trajectories separate with small deviation initially, whereas the deviation increases along with the center angle θ, which finally leads to a certain variation of the wall reflection point and the distance L_w, and the value of L_w decreases with the increase in D_t, as shown in Fig. 19. The results indicate that the model is sensitive to the velocity D_t, and for the present study, the variation of D_t from $0.94D_{CJ}$ and $1.05D_{CJ}$ can make an error of 10 to -8% the distance L_w calculated by the case of $D_t = D_{CJ}$.

6 Conclusions

A semi-analytical model to predict the trajectory of the transverse detonation in re-initiation of weakly unstable detonation wave diffraction was constructed by applying the Chester–Chisnell–Whitham theory. Several key features of cellular detonation wave diffraction that are significant for the model were studied first by numerical simulation with the adaptive mesh refinement code AMROC. The calculation process of the model was presented in detail, and an accuracy verification of the model was conducted. The re-initiation process was analyzed, and the conclusion drawn from pre-

vious research by Nagura et al. [17,18] was explained by adopting the present model.

From the numerical simulations, the position of the local explosion is related to the deviation angle θ_w of the channel. Only at $\theta_w \geq 30°$, the transverse detonation can be generated, and it is shown to derive from a location on the expansion wave front. When $\theta_w \geq 60°$, the horizontal distance s_t from the initial location on the expansion wave front to the channel exit can be predicted by the theory of Edwards et al., which satisfies the relation of $s_t = 5\lambda \cot \alpha$, where λ and α represent the detonation cell width and the horizontal angle of the expansion wave front, respectively. In addition, the velocity of the transverse detonation D_t has an almost equivalent value to the Chapman–Jouguet detonation wave velocity D_{CJ}, and the velocity D_t can be separated into two orthogonal velocity components: the expansion velocity of the diffracted wave front D_v, which is perpendicular to the front, and the relative velocity of the transverse detonation to the diffracted wave front D_h, which is tangent to the front. Moreover, before the transverse detonation reaches the expansion wall, the shape of the decoupled wave front will not be affected by the local explosion and can be predicted by the Chester–Chisnell–Whitham theory.

Based on the numerical observations and the Chester–Chisnell–Whitham theory, a semi-analytical model can be constructed, and the trajectories of the transverse detonation as well as the distances of the wall reflection point L_w can be confirmed, respectively, with various θ_w and initial pressure p_0 under the limitation of $\theta_w \geq 60°$. The results calculated by the model are verified to agree with the present simulation results.

The model denotes that at $150° \geq \theta_w \geq 60°$, the distance L_w varies in a small range of 15–20λ with various θ_w, and the deviation is minimal as θ_w is varied. This trend is considered to be a natural result determined by the three key characteristics of detonation diffraction discussed in this study. Furthermore, it is found that the trajectory of the transverse detonation calculated by the model is self-similar and has dependence only upon the distance s_t. Thus, the relation of $s_t = 5\lambda \cot \alpha$ determines that the parameter L_w/λ can be regarded as constant for the same θ_w and independent of p_0. This characteristic is available for all the weakly unstable detonation waves with regular cellular structures. The analysis which is induced by the model validates the previous finding by Nagura et al. [17,18] and gives a reasonable explanation of the mechanism simultaneously. In addition, the model is found to be sensitive to the velocity D_t, and the deviation of D_t can make a certain error for the calculation result.

Acknowledgements This work is supported by the National Natural Science Foundation of China under Grant Nos. 91441201 and 51776220 and the Natural Sciences and Engineering Research Council of Canada (NSERC). The authors thank A. J. Higgins and the anonymous reviewers whose comments have greatly improved the quality of this manuscript.

References

1. Zeldovich, Y.B.: An experimental investigation of spherical detonation of gases. Sov. Phys. Tech. Phys. **1**, 1689–1713 (1956)
2. Edwards, D., Thomas, G., Nettleton, M.: The diffraction of a planar detonation wave at an abrupt area change. J. Fluid Mech. **95**(1), 79–96 (1979). https://doi.org/10.1017/S002211207900135X
3. Mitrovanov, V.: The diffraction of multifront detonation waves. Sov. Phys. Dokl. **9**, 1055 (1964)
4. Knystautas, R., Lee, J., Guirao, C.: The critical tube diameter for detonation failure in hydrocarbon–air mixtures. Combust. Flame **48**, 63–83 (1982). https://doi.org/10.1016/0010-2180(82)90116-X
5. Murray, S., Lee, J.: On the transformation of planar detonation to cylindrical detonation. Combust. Flame **52**, 269–289 (1983). https://doi.org/10.1016/0010-2180(83)90138-4
6. Arienti, M., Shepherd, J.: A numerical study of detonation diffraction. J. Fluid Mech. **529**, 117–146 (2005). https://doi.org/10.1017/S0022112005003319
7. Pintgen, F., Shepherd, J.: Detonation diffraction in gases. Combust. Flame **156**(3), 665–677 (2009). https://doi.org/10.1016/j.combustflame.2008.09.008
8. Gallier, S., Le Palud, F., Pintgen, F., Mével, R., Shepherd, J.: Detonation wave diffraction in H_2–O_2–Ar mixtures. Proc. Combust. Inst. **36**(2), 2781–2789 (2017). https://doi.org/10.1016/j.proci.2016.06.090
9. Lee, J.H.S.: The Detonation Phenomenon. Cambridge University Press, Cambridge (2008). https://doi.org/10.1017/CBO9780511754708
10. Mehrjoo, N., Zhang, B., Portaro, R., Ng, H., Lee, J.: Response of critical tube diameter phenomenon to small perturbations for gaseous detonations. Shock Waves **24**(2), 219–229 (2014). https://doi.org/10.1007/s00193-013-0491-2
11. Mehrjoo, N., Gao, Y., Kiyanda, C.B., Ng, H.D., Lee, J.H.: Effects of porous walled tubes on detonation transmission into unconfined space. Proc. Combust. Inst. **35**(2), 1981–1987 (2015). https://doi.org/10.1016/j.proci.2014.06.031
12. Xu, H., Mi, X., Kiyanda, C.B., Ng, H.D., Lee, J.H., Yao, C.: The role of cellular instability on the critical tube diameter problem for unstable gaseous detonations. Proc. Combust. Inst. **37**(3), 3545–3553 (2019). https://doi.org/10.1016/j.proci.2018.05.133
13. Whitham, G.: A new approach to problems of shock dynamics Part I Two-dimensional problems. J. Fluid Mech. **2**(2), 145–171 (1957). https://doi.org/10.1017/S002211205700004X
14. Bartlmä, F., Schröder, K.: The diffraction of a plane detonation wave at a convex corner. Combust. Flame **66**(3), 237–248 (1986). https://doi.org/10.1016/0010-2180(86)90137-9
15. Thomas, G., Edwards, D., Lee, J., Knystautas, R., Moen, I., Wei, Y.: Detonation diffraction by divergent channels. Dyn. Explos. Prog. Astronaut. Aeronaut. **106**, 144–154 (1986). https://doi.org/10.2514/5.9781600865800.0144.0154
16. Khasainov, B., Presles, H.N., Desbordes, D., Demontis, P., Vidal, P.: Detonation diffraction from circular tubes to cones. Shock Waves **14**(3), 187–192 (2005). https://doi.org/10.1007/s00193-005-0262-9
17. Nagura, Y., Kasahara, J., Sugiyama, Y., Matsuo, A.: Comprehensive visualization of detonation–diffraction structures and sizes in unstable and stable mixtures. Proc. Combust. Inst. **34**(2), 1949–1956 (2013). https://doi.org/10.1016/j.proci.2012.07.078

18. Nagura, Y., Kasahara, J., Matsuo, A.: Multi-frame visualization for detonation wave diffraction. Shock Waves **26**(5), 645–656 (2016). https://doi.org/10.1007/s00193-016-0663-y
19. Kasahara, J., Kawasaki, A.: Critical condition for detonation diffraction with stable and unstable mixtures. 26th International Colloquium on the Dynamics of Explosions and Reactive Systems, Boston, MA, Paper 963 (2017)
20. Deiterding, R.: Parallel adaptive simulation of multi-dimensional detonation structures. PhD Thesis, Brandenburgischen Technischen Universität Cottbus, Germany (2003)
21. Deiterding, R.: A parallel adaptive method for simulating shock-induced combustion with detailed chemical kinetics in complex domains. Comput. Struct. **87**(11), 769–783 (2009). https://doi.org/10.1016/j.compstruc.2008.11.007
22. Berger, M.J.: Adaptive mesh refinement for hyperbolic partial differential equations. PhD Thesis, Stanford University, California (1982)
23. Yuan, X., Zhou, J., Lin, Z., Cai, X.: Adaptive simulations of detonation propagation in 90-degree bent tubes. Int. J. Hydrog. Energy **41**(40), 18,259–18,272 (2016). https://doi.org/10.1016/j.ijhydene.2016.07.130
24. Yuan, X., Zhou, J., Lin, Z., Cai, X.: Numerical study of detonation diffraction through 90-degree curved channels to expansion area. Int. J. Hydrog. Energy **42**(10), 7045–7059 (2017). https://doi.org/10.1016/j.ijhydene.2017.01.206
25. Cai, X., Deiterding, R., Liang, J., Sun, M., Mahmoudi, Y.: Diffusion and mixing effects in hot jet initiation and propagation of hydrogen detonations. J. Fluid Mech. **836**, 324–351 (2018). https://doi.org/10.1017/jfm.2017.770
26. Miao, S., Zhou, J., Lin, Z., Cai, X., Liu, S.: Numerical study on thermodynamic efficiency and stability of oblique detonation waves. AIAA J. **56**(8), 3112–3122 (2018). https://doi.org/10.2514/1.J056887
27. Peng, H., Huang, Y., Deiterding, R., Luan, Z., Xing, F., You, Y.: Effects of jet in crossflow on flame acceleration and deflagration to detonation transition in methane–oxygen mixture. Combust. Flame **198**, 69–80 (2018). https://doi.org/10.1016/j.combustflame.2018.08.023
28. Yuan, X., Zhou, J., Mi, X., Ng, H.D.: Numerical study of cellular detonation wave reflection over a cylindrical concave wedge. Combust. Flame **202**, 179–194 (2019). https://doi.org/10.1016/j.combustflame.2019.01.018
29. Hairer, E., Wanner, G.: Solving Ordinary Differential Equations II. Stiff and Differential-Algebraic Problems, vol. 14. Springer, Berlin (1991). https://doi.org/10.1007/978-3-662-09947-6
30. Westbrook, C.K.: Chemical kinetics of hydrocarbon oxidation in gaseous detonations. Combust. Flame **46**, 191–210 (1982). https://doi.org/10.1016/0010-2180(82)90015-3
31. Taylor, B., Kessler, D., Gamezo, V., Oran, E.: Numerical simulations of hydrogen detonations with detailed chemical kinetics. Proc. Combust. Inst. **34**(2), 2009–2016 (2013). https://doi.org/10.1016/j.proci.2012.05.045
32. Shi, L., Shen, H., Zhang, P., Zhang, D., Wen, C.: Assessment of vibrational non-equilibrium effect on detonation cell size. Combust. Sci. Technol. **189**(5), 841–853 (2017). https://doi.org/10.1080/00102202.2016.1260561
33. Smirnov, N., Betelin, V., Shagaliev, R., Nikitin, V., Belyakov, I., Deryuguin, Y.N., Aksenov, S., Korchazhkin, D.: Hydrogen fuel rocket engines simulation using LOGOS code. Int. J. Hydrog. Energy **39**(20), 10748–10756 (2014). https://doi.org/10.1016/j.ijhydene.2014.04.150
34. Smirnov, N., Betelin, V., Nikitin, V., Stamov, L., Altoukhov, D.: Accumulation of errors in numerical simulations of chemically reacting gas dynamics. Acta Astronaut. **117**, 338–355 (2015). https://doi.org/10.1016/j.actaastro.2015.08.013
35. Chester, W.: CXLV. The quasi-cylindrical shock tube. Lond. Edinb. Dublin Philos. Mag. J. Sci. **45**(371), 1293–1301 (1954). https://doi.org/10.1080/14786441208561138
36. Chisnell, R.: The motion of a shock wave in a channel, with applications to cylindrical and spherical shock waves. J. Fluid Mech. **2**(3), 286–298 (1957). https://doi.org/10.1017/S0022112057000130
37. Skews, B.W.: The shape of a diffracting shock wave. J. Fluid Mech. **29**(2), 297–304 (1967). https://doi.org/10.1017/S0022112067000825
38. Best, J.: A generalisation of the theory of geometrical shock dynamics. Shock Waves **1**(4), 251–273 (1991). https://doi.org/10.1007/BF01418882
39. Li, H., Ben-Dor, G.: A modified CCW theory for detonation waves. Combust. Flame **113**(1–2), 1–12 (1998). https://doi.org/10.1016/S0010-2180(97)00136-3
40. Ridoux, J., Lardjane, N., Monasse, L., Coulouvrat, F.: Comparison of geometrical shock dynamics and kinematic models for shock-wave propagation. Shock Waves **28**(2), 401–416 (2018). https://doi.org/10.1007/s00193-017-0748-2
41. Peace, J., Lu, F.: On the propagation of decaying planar shock and blast waves through non-uniform channels. Shock Waves (2018). https://doi.org/10.1007/s00193-018-0818-0
42. Ridoux, J., Lardjane, N., Monasse, L., Coulouvrat, F.: Beyond the limitation of geometrical shock dynamics for diffraction over wedges. Shock Waves (2019). https://doi.org/10.1007/s00193-018-00885-w
43. Nettleton, M.: Shock attenuation in a 'gradual' area expansion. J. Fluid Mech. **60**(2), 209–223 (1973). https://doi.org/10.1017/S0022112073000121
44. Sloan, S., Nettleton, M.: A model for the axial decay of a shock wave in a large abrupt area change. J. Fluid Mech. **71**(4), 769–784 (1975). https://doi.org/10.1017/S0022112075002844
45. Sloan, S., Nettleton, M.: A model for the decay of a wall shock in a large abrupt area change. J. Fluid Mech. **88**(2), 259–272 (1978). https://doi.org/10.1017/S0022112078002098